Catalytic Transfer of Magnetism using a Neutral Iridium Phenoxide Complex

Journal:	*Organometallics*
Manuscript ID:	om-2015-00311m.R1
Manuscript Type:	Article
Date Submitted by the Author:	13-May-2015
Complete List of Authors:	Ruddlesden, Amy; University of York, Department of Chemistry Mewis, Ryan; University of York, Department of Chemistry; Manchester Metropolitan University, Division of Chemistry and Environmental Science Green, Gary; University of York, Psychology Whitwood, Adrian; University of York, Chemistry Duckett, Simon; University of York, Chemistry

Catalytic Transfer of Magnetism using a Neutral Iridium Phenoxide Complex

Amy J. Ruddlesden,[a] Ryan E. Mewis,[a] Gary G. R. Green[b], Adrian C. Whitwood[a] and Simon B. Duckett.*[a]

AUTHOR ADDRESS [a] Department of Chemistry, University of York, Heslington, YO10 5DD; Tel: 01904 322564; E-mail: simon.duckett@york.ac.uk, [b] York Neuroimaging Centre, The BiocentreYork, Science Park, Heslington, York, YO10 5NY.

ABSTRACT: A novel neutral iridium carbene complex Ir(κC,O-L_1)(COD) (**1**) [where COD = cyclooctadiene and L_1 = 3-(2-methylene-4-nitrophenolate)-1-(2,4,6-trimethylphenyl) imidazolylidene] with a pendant alkoxide ligand has been prepared and characterized. It contains a strong Ir-O bond and X-ray analysis reveals a distorted square planar structure. NMR spectroscopy reveals dynamic solution state behavior commensurate with rapid seven-membered ring flipping. In CD_2Cl_2 solution, under hydrogen at low temperature, this complex dominates although it exists in equilibrium with a reactive iridium dihydride cyclooctadiene complex. **1** reacts with pyridine and H_2 to form neutral Ir$(H)_2$(κC,O-L_1)$(py)_2$ which also exists in two conformers that differ according to the orientation of the seven-membered metallocycle and whilst its Ir-O bond remains intact, the complex undergoes both pyridine and H_2 exchange. As a consequence, when placed under *para*hydrogen, efficient polarization transfer catalysis (PTC) is observed via the Signal Amplification By Reversible Exchange (SABRE) approach. Due to the neutral character of this catalyst, good hyperpolarization activity is shown in a wide range of solvents for a number of substrates. These observations reflect a dramatic improvement in solvent tolerance of SABRE over that reported for the best PTC precursor IrCl(IMes)(COD). For THF, the associated ^{1}H NMR signal enhancement for the *ortho* proton signal of pyridine shows an increase of 600-fold at 298 K. The level of signal enhancement can be increased further through warming or varying the magnetic field experienced by the sample at the point of catalytic magnetization transfer.

INTRODUCTION

The underlying sensitivity problem in NMR has led to the development and utilization of hyperpolarization methods to address this issue.[1-3] *Para*Hydrogen Induced Polarization[4] (PHIP) is one such method, which produces non-Boltzmann spin populations by the incorporation of *para*hydrogen (*p*-H_2), a nuclear singlet, into unsaturated molecules.[5, 6] This chemical transformation results in increased signal intensity in the corresponding NMR spectra of reaction product nuclei originating from, or coupled to, those that were *p*-H_2 derived nuclei.[7, 8]

Unlike classical PHIP methods, SABRE (Signal Amplification By Reversible Exchange)[9] does not involve incorporation of *p*-H_2 in to the analyte that is to be polarized. Polarization is instead transferred via a *J*-coupling that exists between hydride ligands that are derived from *p*-H_2 and those of the spin-½ analyte nuclei in the polarization transfer catalyst.[9] These catalysts most commonly take the form of cationic iridium complexes, which possess either phosphine[10-13] or N-heterocyclic carbene (NHC) ligands.[14, 15] One of the most successful catalysts to date is based upon [Ir$(H)_2$(IMes)(analyte)$_3$]Cl and it contains magnetically inequivalent but chemically equivalent hydride ligands.[15] This complex has proved active for a wide range of analytes which include pyridine,[15, 16] nicotinamide,[17-19] isoniazid,[20] pyrazinamide,[20] pyrazole[10] and acetonitrile.[13] The magnetic field experienced by the catalyst at the point of polarization transfer is instrumental in determining the amplitude and identity of the created magnetic states.[18] The use of NHC ligands in the catalyst dramatically increased the enhancement levels relative to those with PCy_3.[14, 15, 20, 21] These charged systems contain three analyte molecules and are efficient SABRE catalysts in polar solvents such as methanol with benzene being less effective. In this class of catalyst, SABRE transfer proceeds into the two analyte molecules that are *trans* to hydride ligands. It is ligand exchange, a secondary process, which results in visible hyperpolarization in the analyte molecule in solution.

An alternative catalyst system has been reported that is based on [Ir$(H)_2$(IMes)(PCy_3)(analyte)$_2$]Cl.[13] Now the exemplified analytes are pyridine and acetonitrile. The mixed analyte containing catalyst, [Ir$(H)_2$(IMes)(PCy_3)(pyridine)(CH_3CN)]Cl, which is also charged, proved most effective for SABRE even though it contains a pair of chemically and magnetically inequivalent hydride ligands. These results confirmed that it is possible to block the two axial coordination sites in the SABRE catalyst with non-labile ligands without suppressing activity, whilst retaining a charged system. Species such as [Ir$(H)_2$(IMes)(PCy_3)(pyridine)$_2$]Cl with magnetically inequivalent but chemically equivalent hydride ligands, whilst being directly related to [Ir$(H)_2$(IMes)(analyte)$_3$]Cl, proved less effective due to poor ligand exchange. Herein we present data dealing with the use of a neutral iridium catalyst containing a *cis*-spanning bidentate NHC to mediate polarization transfer from *p*-H_2 to pyridine and nicotinamide. The use of the chelate effect to promote and control catalysis is well exemplified by phosphines,[22] bipyridyl,[23] pincer[24, 25] and pincer carbene ligands.[26-29] We seek to retain a carbene functionality whilst adding a hard anionic oxygen ligand and have selected phenolate because it has found wide use in many inorganic systems.[30-32] Many iridium aliphatic alkoxide systems exist although these

can readily undergo β-hydride elimination.[33, 34] In comparison, phenolate ligands are more stable due to the π-interaction and lack of β-protons. A related system has been shown to act as a hydrogenation catalyst with no elimination of the phenol.[35] Here we employ a phenolate substituted NHC that can coordinate to the same face of the metal to make Ir(κC,O-L_1)(COD) (**1**) [where COD = cyclooctadiene and L_1 = 3-(2-methylene-4-nitrophenolate)-1-(2,4,6-trimethylphenyl) imidazolylidene] in order to achieve this and demonstrate good activity in non-polar solvents whilst retaining optimal catalytic behavior.

RESULTS AND DISCUSSION

Synthesis and Characterization. The synthesis of Ir(κC,O-L_1)(COD) (**1**) via a transmetallation reaction was achieved according to Scheme 1. Occhipinti *et al*. have previously reported the synthesis of the silver carbene complex **AgL_1**[36] and attached it to ruthenium. Here we use a similar route to make **1**. Notably, the precursor, L_1HBr in Scheme 1, shows a broad infrared (IR) signal at ~3000 cm^{-1} for a phenolic O-H stretch as well as signals at 1339 cm^{-1} and 1279 cm^{-1} for the O-H bend and C-OH stretching mode respectively.[36] Complex **1** was prepared in 96% yield and its structure confirmed by NMR, X-ray and mass spectrometry. A peak is present in the IR spectrum of **1** at 1293 cm^{-1} due to a C-OIr stretch.

Scheme 1. Reaction scheme for the formation of Ir(κC,O-L_1)(COD), 1 from AgL_1[36] and $[Ir(COD)Cl]_2$[37].

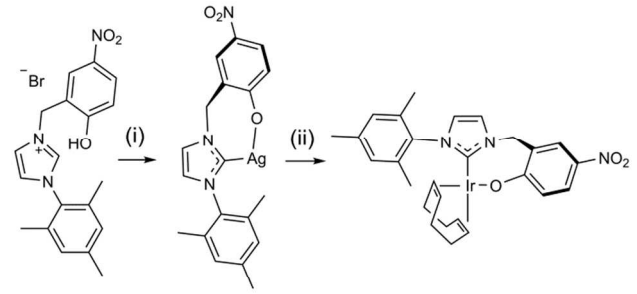

Reagents and conditions: (i) Ag_2O, THF, toluene, reflux, 3 h; (ii) $[Ir(COD)Cl]_2$, THF, r.t., 18 h

Comparison of the NMR data for **1** at 298 K in CD_2Cl_2, with that at 253 K revealed that its proton chemical shifts are strongly temperature dependent. At 298 K, the two aromatic proton resonances for the mesityl group appear as a broad singlet at δ ~7.03 but upon cooling its rotation is hindered and two singlets separate from it, which resonate at δ 7.06 and 6.96. Lineshape analysis[38, 39] of this behavior enabled the activation enthalpy for mesityl group rotation, $\Delta H^{\neq}$, to be estimated as 65.5 ± 3.1 kJ mol^{-1} with the corresponding value for $\Delta S^{\neq}$ being +28.0 ± 10.9 J K^{-1} mol^{-1}. These $\Delta H^{\neq}$ and $\Delta S^{\neq}$ values are commensurate with those expected for an intramolecular ring rotation[40, 41] (see Supplementary Information (SI) for the raw data). We note that similar coalescence effects are also observed when **1** is present in a THF-d_8 solution in accordance with a process where there is little charge separation.[40]

In a separate dynamic process, the two proton resonances of the CH_2 linker are also broadened, in this case into the baseline at 298 K. At 253 K these protons provide two distinct doublets at δ 6.60 and 4.79 that share a common coupling of 13.97 Hz. This behavior is a consequence of the fact that the two CH_2 protons are diastereotopic, due to their differing exo and endo orientations. They become equivalent by inversion of the conformation of the seven-membered ring through ring-flip and alkoxide lone pair inversion.[42] The complexity of the associated NMR spectral changes, and the large chemical shift difference that exists between these resonances, precludes the quantitative analytical assessment of this process through line-shape analysis.

The structure of **1** was further confirmed by X-ray diffraction. Figure 1 shows the corresponding ORTEP plot, determined at 110 K. The crystals employed for this analysis were grown by the slow diffusion of hexane into a dichloromethane solution of **1**. The crystal exhibited both pseudo-merohedral and multi-crystal twinning, see SI for further details. The structure has a distorted square planar geometry around iridium where the corresponding bond angles are close to 90°. **1** can be compared to two related Ir(I) complexes, Ir(IMes)(COD)($OSiMe_3$) containing a siloxide ligand[43] and [Ir(IMes)(COD)(py)]Cl containing a pyridine ligand.[44] These complexes also proved to adopt distorted square planar arrangements. **1** has an Ir-O bond length of 2.067(3) Å which compares well to the value of 2.020(4) Å reported for Ir(IMes)(COD)($OSiMe_3$). For [Ir(IMes)(COD)(py)]Cl the Ir-N bond length is 2.0954(17) Å. The C=C bond of COD which lies *trans* to the phenoxide in **1** is the longest of the series and hence the weakest (1.444(7) Å, compared to 1.407(5) Å for Ir(IMes)(COD)($OSiMe_3$) and 1.399(3) Å for [Ir(IMes)(COD)(py)]Cl). Consequently, the phenoxide ligand in **1** must be the most electron donating ligand of this series and its iridium metal center must therefore be the most electron rich. Due to this increase in electron density at iridium the oxidative addition of H_2 to **1** will be disfavored due to repulsion between it and the electron density provided by the ligands in the five-coordinate transition state.[45]

The bond angle in **1** that exists between $C_{(carbene)}$-Ir-O is 92.88(14)° and smaller than that of $C_{(carbene)}$-Ir-N (94.45(7)°) in [Ir(IMes)(COD)(py)]Cl. This change is a consequence of the chelate effect which acts here to restrict the bond angle but when the freely orientating complex Ir(IMes)(COD)($OSiMe_3$) is compared, the $C_{(carbene)}$-Ir-OSi angle is now compressed to 88.2(2)°. Therefore steric interactions must play a role in determining the shape of these complexes.

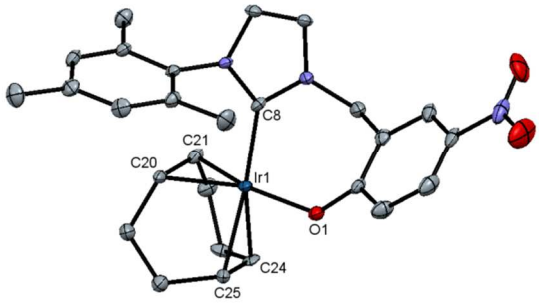

Figure 1. ORTEP plot of **1**. Hydrogens have been omitted for clarity. Selected bond lengths (Å) and angles (°): Ir1-O1, 2.067(3); Ir1-C8, 2.049(4); Ir1-C20, 2.111(5); Ir1-C21, 2.101(5); Ir1-C24, 2.185(4); Ir1-C25, 2.183(4); C20-C21, 1.444(7); C24-C25, 1.393(7); C8-Ir1-O1, 92.88(14).

Reactivity of 1 towards H_2 or pyridine. Upon the addition of *p*-H_2 at 3 bars pressure to a CD_2Cl_2 solution of **1** at 253 K an immediate reaction is observed to take place and the formation of a new dihydride complex (**2**) is indicated (see Scheme 2). This species yields a pair of PHIP polarized hydride resonances at δ −10.84 and −21.51 in the corresponding ^{1}H NMR spectrum where the chemical shift values are diagnostic of sites that lie *trans* to alkene and alkoxide respectively. We note that similar spectral changes have been reported

when H_2 adds to $[Ir(COD)(NCCH_3)(PMe_3)]BF_4$ to form $[Ir(H)_2(COD)(NCCH_3)(PMe_3)]BF_4$.[46] The product of the reaction with **1** is $Ir(H)_2(\kappa C,O\text{-}L_1)(COD)$ (**2**) and it exists in equilibrium with **1** where a steady-state of just 5% conversion is achieved under these conditions.

The very broad hydride and hydrogen signals that are seen in the associated ^1H NMR spectra confirm that the interconversion between **1** and **2** is rapid; upon heating this sample to 303 K the hydride resonances broaden into the baseline of the NMR spectrum. The H_2 / Ir-H exchange process that is indicated by this observation provides a route to destroy the *p*-H_2 that is present in solution because the relaxation times of metal hydride ligands are relatively short.[47, 48] Therefore, despite PHIP being observed when a sample at 243 K is removed from the magnet, shaken and then returned to the magnet for measurement this effect does not last. Furthermore, at 298 K, this pair of hydride signals shows very small levels of PHIP and appears only transiently, thereby confirming that the *p*-H_2 present in solution is consumed very rapidly. We note that significant signal averaging is necessary to observe the hydride resonances of **2** with normal, thermally equilibrated NMR polarization.

Scheme 2. Formation of dihydride 2 from 1.

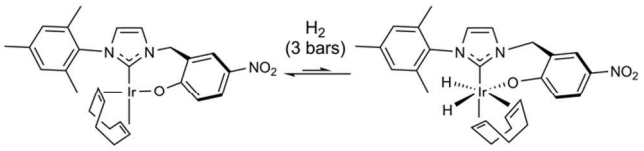

In the corresponding low temperature spectrum, a second pair of very weak hydride signals is observed at 243 K that also exhibit PHIP. These signals are only observed after a considerable number of scans under conditions where the magnetism of the molecules is thermally equilibrated. These new hydride ligand signals appear with just *ca*. 6% of the intensity of those for **2** and are hence too weak to allow the associated product to be characterized. They are likely, however, to arise from a minor isomer of **2** that differs from the main isomer according to the conformation of the seven-membered ring. These signals do not appear in the corresponding high temperature NMR spectrum, presumably due to dynamic averaging between the rapidly interconverting isomers.

Upon adding pyridine to a CD_2Cl_2 solution of **1** the slow displacement of COD is indicated in the resulting ^1H NMR spectrum. However, no clearly identifiable reaction product is observed in this spectrum and decomposition occurs. After 6 days of reaction with pyridine, the subsequent addition of H_2 to the resulting solution leads to the formation of a new dihydride species in 60% yield after a further 3 days of activation.

Formation of 3 from 1 upon addition of pyridine and H_2. In contrast, **1** reacts very slowly and cleanly with H_2 when it is located in a freshly prepared CD_2Cl_2 solution containing pyridine at 298 K to form the same reaction product. We have identified this product as neutral $Ir(H)_2(\kappa C,O\text{-}L_1)(py)_2$, **3** (see Scheme 3) through a series of observations that we now describe. We note that after 24 hours, 40% conversion of a 1.6 x 10^{-5} mol solution of **1** with an 8-fold excess of pyridine under 3 bars pressure of H_2 to **3** is achieved; this reaction goes to completion on a longer timescale.

The infrared spectrum of **3** contains a noteworthy C-O Ir stretch at 1274 cm^{-1} and no evidence for either an OH or OD stretch. The corresponding stretch in **1**, an Ir(I) complex, is 1293 cm^{-1} which suggests that the Ir(III)-alkoxide bond in **3** is strengthened. Furthermore, starting material **1** possesses a strong yellow/orange color when in solution, and this is retained upon activation with pyridine and H_2. UV-Vis analysis of **1** in CH_2Cl_2 reveals the complex yields an absorption band at 405.5 nm with a molar extinction coefficient, ε, of 21060 $dm^3\ mol^{-1}\ cm^{-1}$. Similar analysis of the activated complex, **3**, reveals an absorption band at the slightly higher energy of 398.6 nm with a reduced ε value of 10975 $dm^3\ mol^{-1}\ cm^{-1}$. Interestingly, when the related complex $[Ir(H)_2(IMes)(pyridine)_3]Cl$ is monitored in methanol, no equivalent transition is present, the most prominent feature being a broad blue shifted band at 341.0 nm with an ε of 3413 $dm^3\ mol^{-1}\ cm^{-1}$. The large molar absorptivity values exhibited by **3** are consistent with its intense color and the detection of a charge transfer band.

As expected, COD is released during the formation of **3**, and it proved to be hydrogenated on a slower timescale, first to form COE and then COA [where COE = cyclooctene and COA = cyclooctane] according to NMR analysis. The substitution of COD for pyridine in a related cyclometallated square planar palladium system has been reported[49] as has the hydrogenation of COD in series of related systems.[50-52]

Neutral **3** forms according to Scheme 3 and the alternative zwitterionic Ir-O bond cleaved product $[Ir(H)_2(\kappa C\text{-}L_1\text{-}O^-)(py)_3]^+$ is not observed. At 298 K, the ^1H NMR spectrum of **3** contains two distinct hydride ligands which yield a broad singlet at δ −21.80 for the *trans* pyridine site (H_A) and a sharp doublet at δ −28.90 for the *trans* oxygen site (H_B). Further analysis of these NMR spectra of **3** revealed that upon cooling to 223 K, each hydride signal pair separates into two sets of hydride resonances, at δ −21.40 (H_A) and −29.80 (H_B), and at δ −22.60 ($H_{A'}$) and −29.00 ($H_{B'}$) respectively with relative intensity 83:17. The two pairs of hydride resonances share common −8.9 and −7.3 Hz couplings respectively and are due to two conformers, $\mathbf{3_A}$ and $\mathbf{3_{A'}}$, that result from differing orientations of the seven-membered metallocycle. A ^{15}N-HMQC 2D NMR measurement completed at 233 K, located two signals at δ 258.4 and 240.7 for the equatorial and axial pyridine ligands of the major isomer $\mathbf{3_A}$ respectively. Given that the chemical shift of free pyridine is 303 ppm, and the difference between it and the bound signal has been suggested to be indicative of bond strength, the ligand *trans* to the carbene is more strongly bound.[53] Full characterization data for $\mathbf{3_A}$ at 233 K in CD_2Cl_2 is presented in the SI.

Ligand exchange pathways in $Ir(H)_2(\kappa C,O\text{-}L_1)(py)_2$, 3. When the hydride resonance for H_A of **3** in CD_2Cl_2 is selectively irradiated in an EXSY[54] experiment at 233 K magnetization transfer into only the $H_{A'}$ signal of the second conformer is observed. The rate of this process is 4.00 ± 0.08 s^{-1} and the pair of exchanging hydride ligands remain *trans* to their original partner throughout. Probing the reverse step, by selective irradiation of $H_{A'}$, enabled the rate of transfer of $H_{A'}$ into H_A to be quantified as 19.80 ± 0.33 s^{-1}. This means that the equilibrium constant connecting $\mathbf{3_{A'}}$ and $\mathbf{3_A}$ is 4.95 and we note that it matches that determined by integration.

Exchange of these two hydride ligands into free H_2, or into a site that is *trans* to nitrogen is not observed at 233 K. The latter process, which corresponds to that of isomer interconversion, is however evident at 298 K alongside that of H_2 loss as shown in Scheme 3. In fact, the H_2 loss process proved to be inhibited by the addition of pyridine, while the process of hydride site interchange was unaffected.

Scheme 3. Formation of $Ir(H)_2(\kappa C,O\text{-}L_1)(py)_2$, 3, from 1 with the vacant site represented through the shaded orbital and the purple and magenta hydride ligand labels detailing the hydride interchange processes.

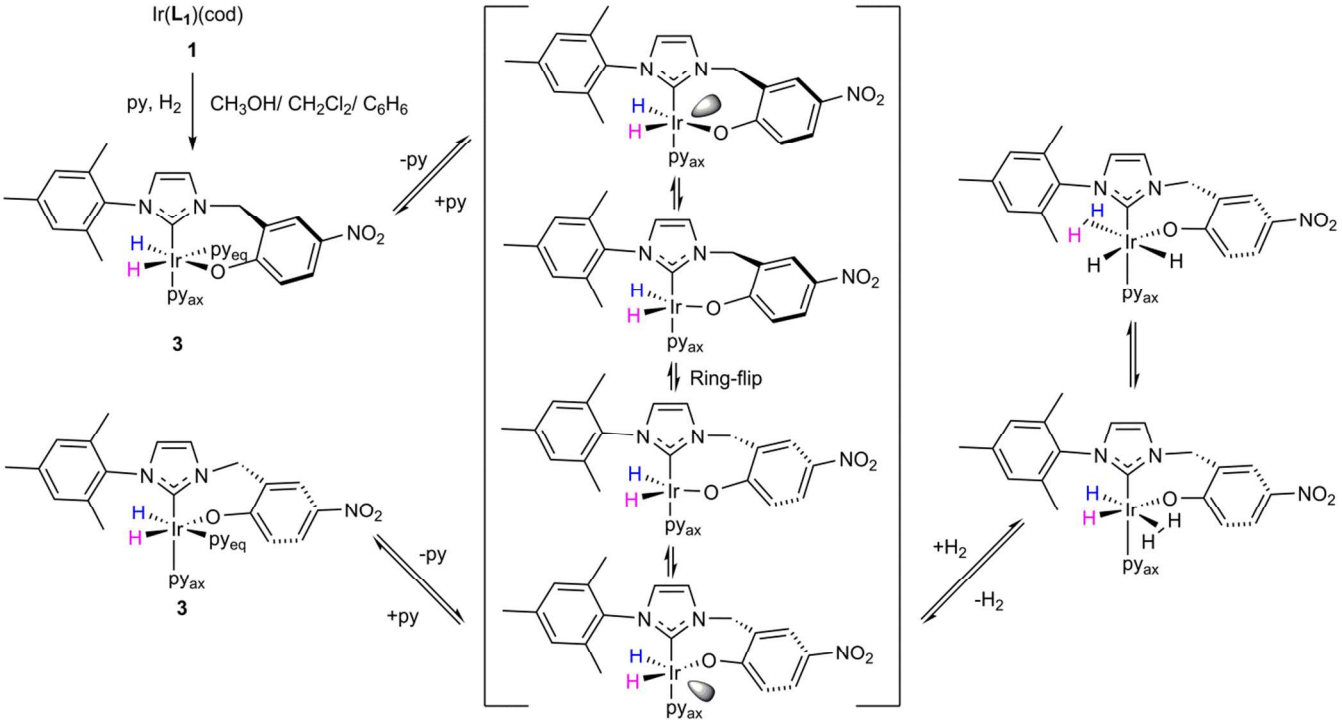

When the corresponding ^{1}H EXSY measurement procedure was used to monitor pyridine exchange in **3** only loss of the equatorial ligand was observed, in a process that followed saturation kinetics. These observations confirm that the loss of pyridine from **3** is therefore dissociative. Furthermore, the resulting 16-electron intermediate must have a trigonal bipyramidal shape, or undergo very rapid hydride site interchange, to equilibrate hydrides H_A and H_B. This is reflected in the fact that the hydride ligand exchange process is unaffected by added pyridine. It can also be concluded that H_2 loss from **3** must therefore proceed after pyridine loss (see Table 1). These deductions are supported by the fact that the rate of H_2 loss for a solution containing a 50-fold excess of pyridine was 0.042 ± 0.002 s^{-1} whilst the corresponding pyridine loss rate was 0.28 ± 0.03 s^{-1}. In addition, a H_2 exchange mechanism based on the transient formation of the related complex $IrCl(H)_2(\eta^2\text{-}H_2)(PPr^i_3)_2$[55, 56] has been described previously. We note that these measurements were relatively straightforward to complete in CD_2Cl_2 as no H/D exchange is evident on the timescales of these measurements.

Table 1. Summary of the specified ligand loss rates from **3** as a function of pyridine concentration in CD_2Cl_2. Data confirms pyridine loss is dissociative and that both hydride site interchange and H_2 loss occurs after this step.

No. of py eq. by NMR ratio	Rate of py loss / s^{-1}	Rate of H_2 loss / s^{-1}
15	0.28 ± 0.03	0.078 ± 0.003
25	0.28 ± 0.03	0.071 ± 0.003
30	0.31 ± 0.01	0.053 ± 0.002
50	0.28 ± 0.03	0.042 ± 0.002

When examined in MeOD-d_4, **1** still reacts with H_2 and pyridine to form **3** in an analogous way to that described in CD_2Cl_2. The hydride ligand resonances of **3** appear at δ –21.62 and –29.22 in this solvent and are hence very similar in value to those in CD_2Cl_2. In this case, 100% conversion of a 7.9 x 10^{-6} mmol solution of **1** is observed after just 24 hours and thus the activation of **1** is much more facile in this polar protic solvent when compared to CD_2Cl_2**.** At 243 K, H/D exchange between the hydrides and the solvent is not observed. However, at 270 K, deuterium exchange from the solvent into the hydride resonances of **3** proceeds with an experimentally determined rate constant of 4.24 x 10^{-5} ± 6 x 10^{-7} s^{-1} and both HD and MeOH-d_3 are formed. At 298 K, the rate constant for H/D exchange increases to 8.19 x 10^{-4} ± 8 x 10^{-6} s^{-1}.

In order to examine the pyridine and H_2 exchange processes more reliably, the solvent MeOH-d_3 was employed. At 298 K, a sample containing 15 eq. of pyridine enabled the observation that the hydride ligand *trans* to the oxygen donor proved to exchange into H_2 with an experimentally determined rate constant of 0.54 ± 0.03 s^{-1}, a $\Delta H^{\neq}$ of 67.5 ± 7 kJ mol^{-1} and a $\Delta S^{\neq}$ of –17.3 ± 25 J K^{-1} mol^{-1}. In contrast, pyridine dissociation at 298 K occurs with a rate constant of 1.33 ± 0.23 s^{-1}, a $\Delta H^{\neq}$ of 71.1 ± 3 kJ mol^{-1} and a $\Delta S^{\neq}$ of 2.4 ± 12 J K^{-1} mol^{-1}. In MeOH-d_3, H_2 loss therefore proceeds at a slower rate than pyridine loss and upon increasing the number of equivalents of pyridine, the rate of H_2 loss is decreased, whilst the rate of pyridine loss remained constant. This is again consistent with the mechanism shown in Scheme 3 and shows that the exchange process remains dissociative in methanol. A mechanism for such an H/D exchange process in a closely related system has been proposed by Brookhart *et al*.[57, 58]

Reaction of 3 with *p*-H_2. Upon addition of *p*-H_2, to a CD_2Cl_2 solution of **1** at 298 K, a single pair of PHIP enhanced hydride signals are observed that are indicative of **3**.[59] The enhanced signal at δ –28.90 that is due to the H_B hydride ligand of **3** and which lies *trans* to oxygen, has a line-width at half height of 14.6 Hz and signal integration confirms a signal enhancement of 346-fold relative to that seen in the normal trace. Its partner appears at δ –21.40 with a half-height width of 45.1 Hz. When the same measurement is made at 268 K or

below, neither the hydride resonances of $\mathbf{3_A}$ or $\mathbf{3_{A'}}$ show PHIP in accordance with the suppression of their exchange with the free H_2 pool.

In order to test for the formation of zwitterionic $[Ir(H)_2(\kappa C\text{-}L_1\text{-}O^-)(py)_3]^+$ we have also examined the formation of **3** when a 1:1 mixture of d_5- and h_5-pyridine is employed. Under these conditions no new PHIP enhanced hydride ligand signals are seen even though related studies on $[Ir(H)_2(IMes)(pyridine)_3]Cl$ would suggest that the presence of the ^2H-label is sufficient to break hydride ligand symmetry and thereby enable it to exhibit PHIP. For these reasons we conclude that the Ir-O bond in **3** is retained throughout these measurements in CD_2Cl_2. Analogous results are observed when the solvent is changed to methanol-d_4 so again the Ir-O bond is retained.

Solvent effects on SABRE catalysis by 3. Evidence for the SABRE effect is also seen in many of the ^1H NMR signals that are observed in these NMR spectra. The simplest experimental procedure to view the SABRE effect involves taking an NMR tube under an atmosphere of *p*-H_2 and shaking it for a set time period in a known magnetic field before rapidly making an NMR observation. We now describe the results of this process in the solvents CD_2Cl_2, benzene-d_6, THF-d_8, methanol-d_4 and ethanol-d_6. We discuss the catalyst activation process and highlight the species that are formed. Table 2 details the performance of **1** under SABRE in the indicated solvents after 2 and 24 days respectively. The hydride ligand that is *trans* to oxygen in **3** always gives rise to a sharp doublet in these ^1H NMR spectra while the resonance for the hydride ligand that lies *trans* to pyridine is considerably broader. This suggests that pyridine loss is possible in accordance with the observations we described earlier in the manuscript.

When a sample containing 0.05 M pyridine and 15 mol% **1** in CD_2Cl_2 is examined in this way, after polarization transfer in a 6.5 x 10^{-3} T field, strong SABRE is visible in the NMR signals observed for free pyridine that is present in solution. This effect manifests itself clearly in the resulting single scan ^1H NMR measurement as a 141-fold enhanced *ortho* pyridine proton resonance when compared to the corresponding signal without polarization transfer. We note that complex **3** is detected as the sole inorganic reaction product in these solutions for periods out to 24 days and that no deuterium exchange with the solvent is evident.

3 also forms cleanly in both benzene-d_6 and THF-d_8 solutions where it is again stable for extended periods of time. We observed, however, that the slow reaction means that significant time is necessary for full activation. When a benzene-d_6 system is examined for SABRE, after 2 days of activation, a 121-fold signal enhancement is seen for the same *ortho* pyridine proton signal under similar conditions. In THF-d_8 the analogous level of signal gain reduces to 98-fold for a similar sample under similar conditions. Despite this drop in SABRE efficiency in THF-d_8, these observations in CD_2Cl_2, benzene-d_6 and THF-d_8, confirm our original hypothesis that neutral **3** is a good SABRE catalyst in a variety of low polarity solvents. When the same systems are examined after 24 days the signal enhancements for the *ortho* protons of pyridine in these samples have now increased to a maximum of 346-fold, 561-fold and 600-fold for CD_2Cl_2, benzene-d_6 and THF-d_8 respectively. This information confirms that while the catalyst takes longer to fully form in these less polar solvents it delivers good activity.

Table 2. Pyridine ^1H NMR signal enhancements produced for a series of 0.05 M pyridine and 15 mol% **1** solutions at 298 K using 3 bars of *p*-H_2 after an activation period of 48 hours and 24 days.

Deuterated solvent	Pyridine ^1H NMR SABRE signal enhancements (fold)					
	48 hours			24 days		
	ortho	*meta*	*para*	*ortho*	*meta*	*para*
Benzene	121	93	56	561	469	253
THF	98	61	49	600	442	265
DCM	141	105	65	346	212	159
Ethanol	86	35	36	282	145	142
Methanol	185	130	82	29	24	18

When the solvent is changed to polar protic methanol or ethanol different behavior is observed. In MeOD-d_4 for a sample containing 0.1 M pyridine and 5 mol% **1**, the initial levels of SABRE that were observed in the ^1H NMR resonances of pyridine are small (~6 fold for the *ortho* ^1H resonances) after shaking in a polarization transfer field (PTF) of 6.5 x 10^{-3} T at 40°C. However, when the same sample is tested 72 hours later, the signal enhancement levels are far greater (178, 96, 52 fold observed for *ortho*, *meta* and *para* ^1H resonances of pyridine respectively). A typical trace is shown in Figure 2. These data confirm our earlier observation that **1** takes a significant time to fully activate. However, upon longer time scales, the level of delivered polarization falls as the pyridine substrate becomes ^2H-labelled; 50% deuteration of the *ortho* proton signal for pyridine was observed after 24 days in methanol-d_4. The analogous deuterium exchange process is seen in ethanol-d_6, but it now proceeds more slowly in accordance with the slower formation of **3**; no deuterium exchange is seen in the non-protic solvents.

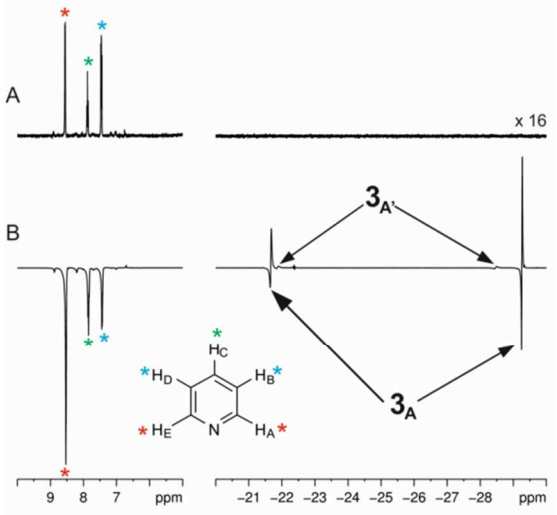

Figure 2. ^1H NMR spectra of a sample containing 0.05 M pyridine and 15 mol% 1 in MeOD-d_4 after; (A) thermal equilibrium at high field; and (B) polarization transfer from *p*-H_2 at 6.5 x10^{-3} T, using a 45° pulse. Pyridine and hydride species are labelled.

In order to demonstrate that the polarization transfer to pyridine observed in these systems arises from SABRE rather than one-proton PHIP, a d_5-pyridine containing solution was also examined. These measurements were completed after shaking the sample in a PTF of 6.5 x 10^{-3} T and involved the application of a 45° excitation pulse. The ^1H NMR signal for residual d_4-pyridine was shown to polarize, delivering an in-phase emission peak at δ 8.56 which rapidly decayed to thermal magnetization over a time course of ~30 s. If this signal was to

be enhanced through the one-proton PHIP effect it should remain enhanced over this period. For this reason we conclude that SABRE is the only polarization transfer pathway operating.[60, 61]

The magnetization transfer process was also probed by OPSY (Only *Para*hydrogen SpectroscopY[62, 63]). This pulse sequence enables the detection of signals that are either derived directly from *p*-H_2 or nuclei that have received polarization from it. Two representative ^{1}H NMR spectra that were recorded after shaking in a PTF of 2 x 10^{-4} T at 0°C or 60°C respectively are shown in Figure 3. It can be readily seen from these NMR spectra that greater polarization transfer is evident at 60°C and that polarization transfer via SABRE into free pyridine occurs. The two NMR spectra are presented in magnitude mode and the signals for pyridine and the hydride resonances of **3** dominate which confirms that they receive visible polarization from *p*-H_2..

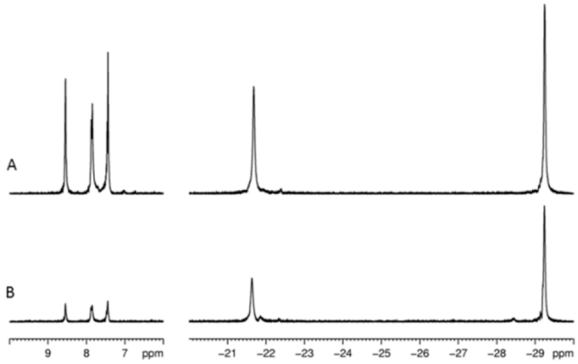

Figure 3. ^{1}H OPSY-dq NMR spectra of a sample containing 0.1 M pyridine and 5 mol% **1** in MeOD-d_4 after polarization transfer from *p*-H_2 at 2 x 10^{-4} T and 60°C (A) or 0°C (B).

SABRE catalysis optimization using 3. In order to optimize the efficiency of polarization transfer in methanol from *p*-H_2 to substrates using **1** a number of conditions have been investigated. These include varying the temperature, the PTF and the catalyst. The most widely used catalyst to date is IrCl(IMes)(COD), **4**.[64,15] When activated with pyridine and H_2, **4** has been reported to form $[Ir(H)_2(IMes)(py)_3]Cl$ which then enables polarization transfer. The route to H_2 addition to **4** is via the formation of [Ir(IMes)(COD)(py)]Cl which actually adds H_2 faster than the precursor IrCl(IMes)(COD). In contrast, **1** takes a significant time to activate due to the analogous indirect reaction pathway being no longer available because of the strong Ir-O bond.

Table 3 displays a series of enhancement data that results from the SABRE of the substrates pyridine and nicotinamide in MeOD-d_4 as a function of temperature and transfer field using both **4** and **1**. It is clear from this table that **4** is the superior room temperature catalyst, delivering in some instances 30 times more signal intensity when compared to that produced by **1**. For **1**, the signal enhancement seen for bulk nicotinamide proton H_A increases by a factor of ~5 on going from 2 x 10^{-4} T to 6.5 x 10^{-4} T at 30°C, and a factor of ~6 at 60°C. This compares with a drop in signal intensity when **4** is employed at the higher temperatures. Now, under transfer at 6.5 x 10^{-4} T, proton H_A of nicotinamide shows better enhancement at 30°C rather than 60°C. These investigations on nicotinamide were conducted because of the recent publications which investigate the biological implications of hyperpolarizing nicotinamide in a move towards developing imaging applications that utilize the SABRE technique.[17-19, 21]

Table 3. Signal enhancements obtained for each of the listed ^{1}H resonances of pyridine and nicotinamide after polarization transfer in fields of either 2 x 10^{-4} T or 6.5 x 10^{-3} T using catalyst **1** or **4** in MeOD-d_4. For proton assignments see the SI.

	Polarization transfer at 2 x 10^{-4} T				Polarization transfer at 6.5 x 10^{-3} T			
	1		**4**		**1**		**4**	
^{1}H resonance	30°C	60°C	30°C	60°C	30°C	60°C	30°C	60°C
Pyridine H_A, H_E	44	72	616	269	116	254	677	474
Pyridine H_B, H_D	20	20	188	35	70	158	182	212
Pyridine H_C	10	20	247	113	28	66	295	205
Nicotinamide H_A	4	7	147	117	20	40	469	393
Nicotinamide H_B	2	2	74	59	15	33	306	242
Nicotinamide H_C	2	4	99	54	6	18	64	55
Nicotinamide H_D	3	5	107	85	20	40	364	293

The effect of temperature is also clearly illustrated in Figure 4. The continued improvement in the activity of **1** with an increase in temperature is associated with an increase in ligand dissociation rate.[15] In contrast, the rate of ligand exchange with **4** actually becomes too rapid for good catalysis upon exceeding 30°C. A full comparison of temperature dependent ^{1}H NMR enhancements for pyridine and nicotinamide in MeOD-d_4 as polarized by **1** and **4** is detailed in the SI.

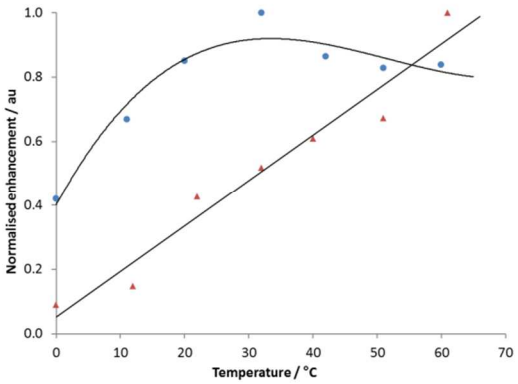

Figure 4. Normalized enhancement of the H_A ^{1}H NMR resonance of nicotinamide after polarization transfer at 6.5 x 10^{-3} T using either **1** (▲) or **4** (●).

Further optimization was achieved by altering the PTF. This study was completed using a polarizer equipped with a vertically aligned coil that is capable of producing a well-defined vertical field between 0.5 x 10^{-4} T and ±1.5 x 10^{-2} T in steps of 0.5 x 10^{-4} T.[15, 18] The four hyperpolarized ^{1}H resonances of nicotinamide resulting from polarization in set fields between −1.5 x 10^{-2} T and +2.5 x 10^{-3} T are illustrated in Figure 5. The maximum signal enhancement proved to be delivered by **1** when the PTF lies between −6.5 x 10^{-3} T and −7.5 x 10^{-3} T for sites H_A, H_B and H_C and their signals all appear in emission. The corresponding *meta* proton (H_C) resonance undergoes two phase changes on moving from −1.5 x 10^{-2} T to −1.25 x 10^{-2} T and −6.5 x 10^{-3} T to −5.0 x 10^{-3} T respectively, and shows relatively weak signal amplification levels. Related observations have been reported for pyridine with **4** and the profiles are remarkably similar even though the two catalysts are very different in their nature.[13]

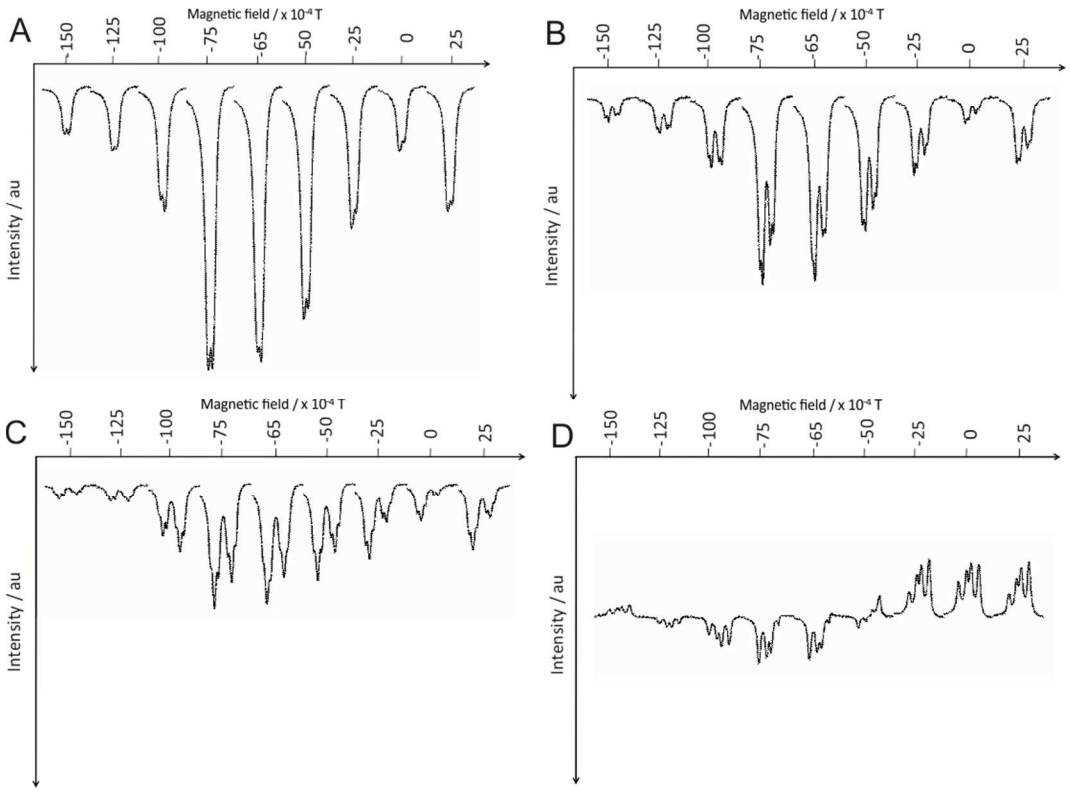

Figure 5. ^{1}H NMR field plots showing the signal intensity of the four ^{1}H (A-H_A, B-H_D, C-H_B, D-H_C) resonances of nicotinamide over the range of −1.5 x 10^{-2} T to +2.5 x 10^{-3} T.

Two other substrates that have been shown to polarize using **4** for SABRE in methanol include quinoline[65] and nicotine.[21] We have therefore examined these substrates using **1** in benzene as this is one of the most efficient solvent systems for this neutral catalyst. Both compounds show enhanced signals, with polarization transfer to nicotine being more efficient than quinolone. Nicotine exhibits a total proton enhancement of 360-fold across the four aromatic proton sites with quinolone showing a 54-fold increase across six of its proton sites. This shows that the use of specially designed catalysts in non-polar solvents could prove very important for identifying low concentration analytes in solution via the SABRE approach.

CONCLUSIONS

The iridium precatalyst Ir(κC,O-L_1)(COD) (**1**) which contains a phenolate substituted NHC has been synthesized and shown to act as a SABRE catalyst precursor in the five solvents, dichloromethane, benzene, tetrahydrofuran, methanol and ethanol. This overcomes the current low polarity solvent limitations shown by existing SABRE catalysts. **1** contains strong Ir-O and Ir-NHC bonds which are preserved in all of these solvents and the chelate effect acts to create a seven-membered metallocycle that adopts two interconverting conformations in solution because of the non-linearity of the Ir-O-C bond. In addition, the square planar catalyst precursor **1**, exhibits a strong charge transfer transition at 398 nm.

We have shown that **1** and H_2 exist in equilibrium with dihydride **2** at low temperature in CD_2Cl_2 solution. The hydride resonances of this product exhibit PHIP in the associated ^{1}H NMR spectra. **2** is an example of an unusual M$(H)_2$(alkene) intermediate, for which other related complexes have been implicated in hydrogenation catalysis in many systems.[66, 67] Upon warming **1** in the presence of pyridine and H_2 in the five described solvents, slow conversion into neutral **3**, Ir$(H)_2$(κC,O-L_1)$(py)_2$ is observed. The stepwise hydrogenation of COD, first into COE and then COA is also evident upon studying this reaction at 298 K.

Neutral **3** has been shown to undergo the dissociative loss of pyridine, according to Scheme 3, prior to H_2 exchange but no evidence for the reductive elimination of the *cis* IrO and IrH groups is observed even though the corresponding alcohol would be expected to be stable. The pyridine and H_2 ligand loss processes enables the incorporation of *p*-H_2 into **3** and thereby facilitates its action as a good SABRE catalyst.

In methanol, the formation of **3** proceeds cleanly with no evidence being observed for zwitterionic [Ir$(H)_2$(κC-L_1-O^-)$(py)_2(CD_3OD)]^+$ or [Ir$(H)_2$(κC-L_1-O^-)$(py)_3]^+$ in solution. The ligand exchange rates for substrate dissociation and H_2 loss have been determined in MeOH-d_3, and both increase with temperature. The H_2 loss process has been suggested to proceed via Ir$(H)_2(H_2)$(κC,O-L_1)(py) as shown in Scheme 3. The associated activation parameters for the H_2 loss process, $\Delta H^{\neq}$ and $\Delta S^{\neq}$ are 67.5 ± 7 kJ mol^{-1} and −17.3 ± 25 J K^{-1} mol^{-1} respectively. In contrast, pyridine dissociation which precedes H_2 loss occurs with a $\Delta H^{\neq}$ of 71.1 ± 3 kJ mol^{-1} and a $\Delta S^{\neq}$ of 2.4 ± 12 J K^{-1} mol^{-1}. The entropy term for this latter reaction is smaller than expected for a dissociative exchange pathway and may reflect an early transition state or a reduction in the conformational freedom of the seven-membered ring.

Nevertheless, when **3** is monitored for activity as a polarization transfer catalyst good levels of hyperpolarization are seen in a range of substrates when utilizing the low polarity solvents, CD_2Cl_2, benzene-d_6 and THF-d_8 that find widespread use in NMR spectroscopy. For example, in THF, the *ortho* proton of the substrate pyridine shows an impressive 600-fold enhancement which equates to 2% polarization level. Furthermore, the level of PTC was found to be PTF dependent,

and in methanol, the best single spin polarization resulted from transfer at a field strength of between −6.5 x 10^{-3} T and −7.5 x 10^{-3} T. When PTC by **3** in methanol is compared to that achieved by $[Ir(H)_2(IMes)(py)_3]Cl$, whilst lower catalyst efficiency is observed, the enhancement levels are still commensurate with significant time savings in both NMR and MRI measurements. Superior catalysis is, however, found in benzene using **1** and similar signal enhancements are seen in dichloromethane albeit with a different catalyst species present to that described previously for **4**.

The range of substrates exemplified includes pyridine, quinoline and nicotine in order to demonstrate the wider utility of this catalyst in non-polar solvents. We note that catalyst activation takes on average 5 days in these relatively non-polar solvents but over 500-fold *ortho* proton enhancement values for pyridine result. These enhancement levels can be improved further still by warming and using an optimized PTF. We therefore expect derivatives of this neutral catalyst to dramatically widen the applicability of SABRE for NMR measurements in the future, and we are now seeking to prepare a precatalyst such as $Ir(\kappa C,O\text{-}L_1)(COE)_2$ which may activate rapidly whilst retaining both the air stability and efficiency of **1**.

EXPERIMETNAL PROCEEDURES

Methods and equipment. All experimental procedures were performed under an atmosphere of either dinitrogen or argon, using standard Schlenk line techniques or an MBraun Unilab glovebox, unless otherwise stated. General solvents for synthetic chemistry were dried using an Innovative Technology anhydrous solvent engineering system or were distilled from an appropriate drying agent under N_2 as necessary. Deuterated solvents (methanol- d_4, methanol- d_3, $CDCl_3$, CD_2Cl_2, benzene- d_6, THF- d_8) were obtained from Sigma-Aldrich and Cambridge Isotope Laboratories (ethanol- d_6) and used as supplied. NMR measurements were made on a Bruker Avance III series 400 MHz NMR spectrometer (^{1}H at 400.13 MHz, ^{13}C at 100 MHz) and a 500 MHz NMR spectrometer (^{1}H at 500.13 MHz, ^{13}C at 125.77 MHz). NMR samples were made up in Young's tap equipped 5 mm NMR tubes. *Para*hydrogen (p-H_2) was prepared by cooling hydrogen gas over charcoal in a copper block at 30 K. COSY, HMQC and EXSY[54] pulse sequences were used as previously described. Polarization transfer experiments are described in the supplementary.

X-ray. Single crystals of $C_{27}H_{30}Ir_{1.04}N_3O_3$ (1) were grown from slow diffusion of hexane into a DCM solution of 1. A suitable crystal was selected and diffraction data were collected at 110 K on an Oxford Diffraction SuperNova diffractometer with Cu-K_α radiation (λ = 1.54184 Å) using an EOS CCD camera. The crystal was cooled with an Oxford Instruments Cryojet. Diffractometer control, data collection, initial unit cell determination, frame integration and unit-cell refinement was carried out with "Crysalis" (CrysAlisPro, Oxford Diffraction Ltd. Version 1.171.34.40). Face-indexed absorption corrections were applied using spherical harmonics, implemented in SCALE3 ABSPACK scaling algorithm (Empirical absorption correction using spherical harmonics, implemented in SCALE3 ABSPACK scaling algorithm within CrysAlisPro software, Oxford Diffraction Ltd. Version 1.171.34.40). OLEX2[68] was used for overall structure solution, refinement and preparation of computer graphics and publication data. Within OLEX2, the algorithm used for structure solution was direct methods,[69] within SHELXS. Refinement by full-matrix least-squares used the SHELXL algorithm within OLEX2. All non-hydrogen atoms were refined anisotropically. Hydrogen atoms were placed using a "riding model" and included in the refinement at calculated positions.

The crystal exhibited both merohedral and multi-crystal twinning. Only one form of twinning can be modelled. Modelling the merohedral twinning gave a statistically better result than the multi-crystal twin model. For the merohedral twinning, a twin matrix of -1 0 0 0 -1 0 0 0 1 was used with a BASF of 0.0863(5). This left large residual density of 8 e Å^{-3} presumably due to the alternative site of iridium from the multi-crystal twinning. This was accounted for by adding a partially occupied iridium with a refined occupancy of 0.0418(12), all other atoms from this minor form were too weak to be modelled. Inclusion of the partial iridium gave a significant improvement in the structure quality (R_1 [I>=2σ (I)] from 4.22 to 3.45%, wR_2 [All data] from 10.06 to 7.01%, residual density from 8.08 to 1.81 e Å^{-3}).

Synthesis of 1-(2,4,6-trimethylphenyl)-1H-imidazole.[70] Glacial acetic acid (10 ml), aqueous formaldehyde (3 ml, 37 wt %, 40 mmol) and aqueous glyoxal (4.6 ml, 40 wt %, 40 mmol) were added to a round bottom flask and heated at 70°C. A solution of glacial acetic acid (10 ml), ammonium acetate (3.08 g, 40 mmol, in 2 ml water) and mesitylamine (5.6 ml, 40 mmol) was added dropwise to the flask over a period of 30 min. The resulting solution was continuously stirred and heated for 18 h. The reaction mixture was cooled to room temperature and was added dropwise to a stirred solution of sodium hydrogen carbonate (29.4 g in 300 ml water). The product formed a precipitate which was filtered off and washed with water before being allowed to air dry. The brown solid was dissolved in the minimal amount of ethyl acetate and placed in a freezer o/n whereupon the required product crystallised and was isolated via filtration (4.36 g, yield 59 %); ^{1}H NMR [$CDCl_3$, 400 MHz] δ 7.44 (s, 1H, $CH_{imidazole}$), 7.24 (s, 1H, $CH_{imidazole}$), 6.98 (s, 2H, 2x$CH_{mesityl}$), 6.90 (s, 1H, $CH_{imidazole}$), 2.35 (s, 3H, CH_3), 2.00 (s, 6H, 2xCH_3); ^{13}C{^{1}H} NMR [$CDCl_3$] δ 138.8, 137.5, 135.4, 133.4, 129.5, 129.0, 120.1, 21.0 (CH_3), 17.3 (2xCH_3); MS [ESI] m/z 187.0 $(M+H)^+$

Synthesis of 3-(2-methylene-4-nitrophenol)-1-(2,4,6-trimethylphenyl) imidazolium bromide, L_1HBr.[36] 1-(2,4,6-trimethylphenyl)-1H-imidazole (0.61 g, 3.3 mmol) and 2-hydroxy-5-nitrobenzyl bromide (0.76 g, 3.3 mmol) were dissolved in toluene (8 ml). The resulting mixture was refluxed for 18 h and then the solution was cooled to room temperature. The precipitate was collected via vacuum filtration and was washed with diethyl ether (1.25 g, yield 91 %); ^{1}H NMR [DMSO, 400 MHz] δ 11.81 (s, 1H, O*H*), 9.55 (s, 1H, $CH_{imidazole}$), 8.39 (d, 1H, ^4J(HH) = 2.55 Hz, $CH_{aromatic}$), 8.22 (dd, 1H, ^4J(HH) = 2.55 Hz, ^3J(HH) = 9.04 Hz, $CH_{aromatic}$), 8.05 (s, 1H, $CH_{imidazole}$), 7.94 (s, 1H, $CH_{imidazole}$), 7.15 (s, 2H, 2x$CH_{mesityl}$), 7.09 (d, 1H, ^3J(HH) = 9.04 Hz, $CH_{aromatic}$), 5.53 (s, 2H, CH_2), 2.33 (s, 3H, CH_3), 2.01 (s, 6H, 2xCH_3); ^{13}C{^{1}H} NMR [DMSO, 500 MHz] δ 163.3 ($C_{aromatic}$), 141.2 ($C_{aromatic}$), 140.3 ($C_{aromatic}$), 139.1 ($CH_{imidazole}$), 135.2 ($C_{aromatic}$), 132.0 ($C_{aromatic}$), 130.1 (2x$CH_{mesityl}$), 128.1 ($CH_{aromatic}$), 127.9 ($CH_{aromatic}$), 125.0 ($CH_{imidazole}$), 124.1 ($CH_{imidazole}$), 122.2 ($C_{aromatic}$), 116.7 ($CH_{aromatic}$), 49.2 (CH_2), 21.5 (CH_3), 17.7 (2xCH_3); MS [ESI] m/z 338.1 $(M\text{-}Br)^+$

Synthesis of silver(II) 3-(2-methylene-4-nitrophenolate)-1-(2,4,6-trimethylphenyl)imidazolylidene, AgL_1.[36] L_1 (500 mg, 1.2 mmol), silver (I) oxide (569.4 mg, 2.5 mmol) and 4Å molecular sieves (1.12 g) were added to a Schlenk flask under a nitrogen atmosphere. Dried THF (8.5 ml) and toluene (8.5

ml) were added to the flask and the reaction mixture was stirred at reflux for 3 h. Once cooled to room temperature, the mixture was diluted with dichloromethane (80 ml), filtered through a pad of celite and washed through with dichloromethane (2 x 5 ml). The solvent was removed under pressure to produce a yellow solid (0.45 g, yield 85%); ^{1}H NMR [$CDCl_3$, 400 MHz] δ 8.16 (s br, 1H, $CH_{aromatic}$), 7.78 (s br, 1H, $CH_{aromatic}$), 7.38 (s br, 1H, $CH_{aromatic}$), 7.01 (s br, 2H, $2xCH_{mesityl}$), 6.99 (s br, 1H, $CH_{aromatic}$), 5.84 (s br, 1H, $CH_{aromatic}$), 5.27 (s br, 2H, CH_2), 2.42 (s, 3H, CH_3), 1.96 (s br, 6H, $2xCH_3$); ^{13}C{^{1}H} NMR [$CDCl_3$] δ 174.7, 139.6, 137.2, 135.2, 134.5, 129.2 ($2xCH_{mesityl}$), 127.2 ($CH_{aromatic}$), 126.8 ($CH_{aromatic}$), 124.4, 122.2, 121.9 ($CH_{aromatic}$), 121.5 ($CH_{aromatic}$), 50.3 (CH_2), 21.4 (CH_3), 17.9 ($2xCH_3$); MS [ESI] m/z 783 (Ag dimer, protonated phenol groups)

Synthesis of iridium(I) (3-(2-methylene-4-nitrophenolate)-1-(2,4,6-trimethylphenyl)imidazolylidene) (cyclooctadiene), 1.[37] AgL_1 (170 mg, 0.38 mmol) and $[Ir(COD)Cl]_2$ (129 mg, 0.19 mmol) were added to a Schlenk flask, which was evacuated and filled with nitrogen. Dry THF (12 ml) was added to the flask and the reaction mixture was stirred overnight at room temperature. The mixture was diluted with DCM, filtered through a pad of celite then purified by column chromatography (silica, DCM:acetone 80:20). It was evaporated to dryness to produce an orange/brown powder (0.23 g, yield 96 %); ^{1}H NMR [CD_2Cl_2, 500 MHz, 298 K] δ 8.17 (d, 1H, ^{4}J(HH) = 3.05 Hz, $CH_{aromatic}$), 7.96 (dd, 1H, ^{4}J(HH) = 3.05 Hz, ^{3}J(HH) = 9.28 Hz, $CH_{aromatic}$), 7.14 (d, 1H, ^{3}J(HH) = 1.94 Hz, $CH_{imidazole}$), 7.03 (s, br, 2H, $2xCH_{mesityl}$), 6.72 (d, 1H, ^{3}J(HH) = 1.94 Hz, $CH_{imidazole}$), 6.60 (s v. br, 1H, CH_2 linker), 6.57 (d, 1H, ^{3}J(HH) = 9.28 Hz, $CH_{aromatic}$), 4.79 (s v. br, 1H, CH_2 linker), 4.40 (s, v. br, 2H, $2xCH_{COD}$), 3.30 (s v. br, 1H, CH_{COD}), 2.45 (s v. br, 1H, CH_{COD}), 2.39 (s, 3H, CH_3), 2.09 (s br, 4H, $CH_{2\ COD}$), 2.03 (s br, 6H, $2xCH_3$), 1.58 (s br, 4H, $CH_{2\ COD}$); ^{1}H NMR [CD_2Cl_2, 500 MHz, 253 K] δ 8.18 (d, 1H, ^{4}J(HH) = 3.01 Hz, $CH_{aromatic}$), 7.96 (dd, 1H, ^{4}J(HH) = 3.01 Hz, ^{3}J(HH) = 9.24 Hz), 7.14 (d, 1H, ^{3}J(HH) = 1.87 Hz, $CH_{imidazole}$), 7.06 (s, 1H, $CH_{mesityl}$), 6.96 (s, 1H, $CH_{mesityl}$), 6.72 (d, 1H, ^{3}J(HH) = 1.87 Hz, $CH_{imidazole}$), 6.60 (d, 1H, ^{2}J(HH) = 14.02 Hz, CH_2 linker), 6.55 (d, 1H, ^{3}J(HH) = 9.24 Hz, $CH_{aromatic}$), 4.79 (d, 1H, ^{2}J(HH) = 14.02 Hz, CH_2 linker), 4.42 (m, 1H, CH_{COD}), 4.26 (m, 1H, CH_{COD}), 3.27 (m, 1H, CH_{COD}), 2.41 (m, 1H, CH_{COD}), 2.36 (s, 3H, CH_3), 2.20 – 2.00 (m, 4H, $2xCH_{2\ COD}$), 2.07 (s, 3H, CH_3), 1.96 (s, 3H, CH_3), 1.68 – 1.53 (m, 4H, $2xCH_{2\ COD}$); ^{13}C{^{1}H} NMR [CD_2Cl_2, 500 MHz, 253 K] δ 175.7 (C-OIr), 175.1 (C-Ir), 139.0 ($C_{aromatic}$), 136.1 ($C_{aromatic}$), 135.5 ($C_{aromatic}$), 134.4 ($C_{aromatic}$), 134.0 ($C_{aromatic}$), 129.1 ($CH_{aromatic}$), 128.4 ($CH_{aromatic}$), 127.0 ($CH_{aromatic}$), 126.3 ($CH_{aromatic}$), 123.4 ($CH_{imidazole}$), 123.2 ($C_{aromatic}$), 121.5 ($CH_{aromatic}$), 119.6 ($CH_{imidazole}$), 84.7 (CH), 84.6 (CH), 51.2 (CH_2), 49.7 (CH), 48.3 (CH), 34.5 (CH_2), 33.8 (CH_2), 28.9 (CH_2), 28.4 (CH_2), 21.0 (CH_3), 18.7 (CH_3), 17.6 (CH_3); MS [ESI] m/z 636.19. Anal. Calcd for $C_{27}H_{30}N_3O_3Ir$ (M_r = 636.77): C, 50.93; H, 4.75; N, 6.60. Found: C, 50.64; H, 4.52; N, 6.14.

ASSOCIATED CONTENT

Supporting Information

Experimental details, exchange rate data, activation parameters, crystal structure data, UV-vis and IR analysis, SABRE analysis of pyridine in different solvents, ^{1}H and ^{13}C hyperpolarized spectra of nicotinamide and pyridine and enhancement vs temperature graphs. This material is available free of charge via the Internet at http://pubs.acs.org.

AUTHOR INFORMATION

Corresponding Author

*simon.duckett@york.ac.uk

Present Addresses

Ryan E. Mewis is now a Lecturer in Inorganic Chemistry at Manchester Metropolitan University.

Author Contributions

The manuscript was written through contributions of all authors. All authors have given approval to the final version of the manuscript. The authors declare no competing financial interests.

ACKNOWLEDGMENT

We acknowledge the Nuffield Foundation for an undergraduate bursary for AJR (URB/39689), Bruker Biospin, the University of York, the EPSRC (grant no. EP/G009546/1) and the Wellcome Trust and Wolfson Foundation (092506 and 098335) for their generous funding.

REFERENCES

(1) Ardenkjaer-Larsen, J. H.; Fridlund, B.; Gram, A.; Hansson, G.; Hansson, L.; Lerche, M. H.; Servin, R.; Thaning, M.; Golman, K., *Proc. Natl. Acad. Sci. U. S. A.* **2003,** *100*, 10158-10163.

(2) Nikolaou, P.; Coffey, A. M.; Walkup, L. L.; Gust, B. M.; Whiting, N.; Newton, H.; Barcus, S.; Muradyan, I.; Dabaghyan, M.; Moroz, G. D.; Rosen, M. S.; Patz, S.; Barlow, M. J.; Chekmenev, E. Y.; Goodson, B. M., *Proc. Natl. Acad. Sci. U. S. A.* **2013,** *110*, 14150-14155.

(3) Acosta, R. H.; Blumler, P.; Munnemann, K.; Spiess, H. W., *Prog. Nucl. Magn. Reson. Spectrosc.* **2012,** *66*, 40-69.

(4) Eisenschmid, T. C.; Kirss, R. U.; Deutsch, P. P.; Hommeltoft, S. I.; Eisenberg, R.; Bargon, J.; Lawler, R. G.; Balch, A. L., *J. Am. Chem. Soc.* **1987,** *109*, 8089-8091.

(5) Bowers, C. R.; Weitekamp, D. P., *J. Am. Chem. Soc.* **1987,** *109*, 5541-5542.

(6) Pravica, M. G.; Weitekamp, D. P., *Chem. Phys. Lett.* **1988,** *145*, 255-258.

(7) Natterer, J.; Bargon, J., *Prog. Nucl. Magn. Reson. Spectrosc.* **1997,** *31*, 293-315.

(8) Green, R. A.; Adams, R. W.; Duckett, S. B.; Mewis, R. E.; Williamson, D. C.; Green, G. G. R., *Prog. Nucl. Magn. Reson. Spectrosc.* **2012,** *67*, 1-48.

(9) Adams, R. W.; Duckett, S. B.; Green, R. A.; Williamson, D. C.; Green, G. G. R., *J. Chem. Phys.* **2009,** *131*.

(10) Dücker, E. B.; Kuhn, L. T.; Münnemann, K.; Griesinger, C., *J. Magn. Reson.* **2012,** *214*, 159-165.

(11) Atkinson, K. D.; Cowley, M. J.; Duckett, S. B.; Elliott, P. I. P.; Green, G. G. R.; Lopez-Serrano, J.; Khazal, I. G.; Whitwood, A. C., *Inorg. Chem.* **2009,** *48*, 663-670.

(12) Atkinson, K. D.; Cowley, M. J.; Elliott, P. I. P.; Duckett, S. B.; Green, G. G. R.; Lopez-Serrano, J.; Whitwood, A. C., *J. Am. Chem. Soc.* **2009,** *131*, 13362-13368.

(13) Fekete, M.; Bayfield, O.; Duckett, S. B.; Hart, S.; Mewis, R. E.; Pridmore, N.; Rayner, P. J.; Whitwood, A., *Inorg. Chem.* **2013,** *52*, 13453-13461.

(14) van Weerdenburg, B. J. A.; Gloggler, S.; Eshuis, N.; Engwerda, A. H. J.; Smits, J. M. M.; de Gelder, R.; Appelt, S.; Wymenga, S. S.; Tessari, M.; Feiters, M. C.; Blumich, B.; Rutjes, F. P. J. T., *Chem. Commun.* **2013,** *49*, 7388-7390.

(15) Cowley, M. J.; Adams, R. W.; Atkinson, K. D.; Cockett, M. C. R.; Duckett, S. B.; Green, G. G. R.; Lohman, J. A. B.; Kerssebaum, R.; Kilgour, D.; Mewis, R. E., *J. Am. Chem. Soc.* **2011,** *133*, 6134-6137.

(16) Barskiy, D. A.; Kovtunov, K. V.; Koptyug, I. V.; He, P.; Groome, K. A.; Best, Q. A.; Shi, F.; Goodson, B. M.; Shchepin, R. V.; Truong, M. L.; Coffey, A. M.; Waddell, K. W.; Chekmenev, E. Y., *ChemPhysChem* **2014,** *15*, 4100-4107.
(17) Hoevener, J.-B.; Schwaderlapp, N.; Borowiak, R.; Lickert, T.; Duckett, S. B.; Mewis, R. E.; Adams, R. W.; Burns, M. J.; Highton, L. A. R.; Green, G. G. R.; Olaru, A.; Hennig, J.; von Elverfeldtt, D., *Anal. Chem.* **2014,** *86*, 1767-1774.
(18) Mewis, R. E.; Atkinson, K. D.; Cowley, M. J.; Duckett, S. B.; Green, G. G. R.; Green, R. A.; Highton, L. A. R.; Kilgour, D.; Lloyd, L. S.; Lohman, J. A. B.; Williamson, D. C., *Magn. Reson. Chem.* **2014,** *52*, 358-69.
(19) Truong, M. L.; Shi, F.; He, P.; Yuan, B.; Plunkett, K. N.; Coffey, A. M.; Shchepin, R. V.; Barskiy, D. A.; Kovtunov, K. V.; Koptyug, I. V.; Waddell, K. W.; Goodson, B. M.; Chekmenev, E. Y., *J. Phys. Chem. B* **2014,** *118*, 13882-13889.
(20) Zeng, H.; Xu, J.; Gillen, J.; McMahon, M. T.; Artemov, D.; Tyburn, J.-M.; Lohman, J. A. B.; Mewis, R. E.; Atkinson, K. D.; Green, G. G. R.; Duckett, S. B.; van Zijl, P. C. M., *J. Magn. Reson.* **2013,** *237*, 73-78.
(21) Adams, R. W.; Aguilar, J. A.; Atkinson, K. D.; Cowley, M. J.; Elliott, P. I. P.; Duckett, S. B.; Green, G. G. R.; Khazal, I. G.; Lopez-Serrano, J.; Williamson, D. C., *Science* **2009,** *323*, 1708-1711.
(22) Chikkali, S. H.; van der Vlugt, J. I.; Reek, J. N. H., *Coord. Chem. Rev.* **2014,** *262*, 1-15.
(23) Espinet, P.; Soulantica, K., *Coord. Chem. Rev.* **1999,** *193-5*, 499-556.
(24) Zhang, W.-H.; Chien, S. W.; Hor, T. S. A., *Coord. Chem. Rev.* **2011,** *255*, 1991-2024.
(25) Selander, N.; Szabo, K. J., *Chem. Rev.* **2011,** *111*, 2048-2076.
(26) Pugh, D.; Danopoulos, A. A., *Coord. Chem. Rev.* **2007,** *251*, 610-641.
(27) Lin, I. J. B.; Vasam, C. S., *Coord. Chem. Rev.* **2007,** *251*, 642-670.
(28) Douthwaite, R. E., *Coord. Chem. Rev.* **2007,** *251*, 702-717.
(29) Diez-Gonzalez, S.; Marion, N.; Nolan, S. P., *Chem. Rev.* **2009,** *109*, 3612-3676.
(30) Fu, R.; Bercaw, J. E.; Labinger, J. A., *Organometallics* **2011,** *30*, 6751-6765.
(31) Noshiranzadeh, N.; Emami, M.; Bikas, R.; Slepokura, K.; Lis, T., *Polyhedron* **2014,** *72*, 56-65.
(32) Kozlowska, A.; Dranka, M.; Zachara, J.; Pump, E.; Slugovc, C.; Skowerski, K.; Grela, K., *Chem.-Eur. J.* **2014,** *20*, 14120-14125.
(33) Blum, O.; Milstein, D., *J. Organomet. Chem.* **2000,** *593*, 479-484.
(34) Zhao, J.; Hesslink, H.; Hartwig, J. F., *J. Am. Chem. Soc.* **2001,** *123*, 7220-7227.
(35) Weinberg, D. R.; Hazari, N.; Labinger, J. A.; Bercaw, J. E., *Organometallics* **2010,** *29*, 89-100.
(36) Occhipinti, G.; Jensen, V. R.; Tornroos, K. W.; Froystein, N. A.; Bjorsvik, H. R., *Tetrahedron* **2009,** *65*, 7186-7194.
(37) Herde, J. L.; Lambert, J. C.; Senoff, C. V.; Cushing, M. A., Cyclooctene and 1,5-Cyclooctadiene Complexes of Iridium(I). In *Inorg. Syn.*, John Wiley & Sons, Inc.2007; pp 18-20.
(38) Bell, H. M., *J. Chem. Educ.* **1976,** *53*, 665.
(39) Harris, D. C., *J. Chem. Educ.* **1998,** *75*, 119-121.
(40) Kappert, W.; Sander, W.; Landgrafe, C., *Liebigs Ann.-Recl.* **1997**, 2519-2524.
(41) Coluccini, C.; Grilli, S.; Lunazzi, L.; Mazzanti, A., *J. Org. Chem.* **2003,** *68*, 7266-7273.
(42) Peng, H. M.; Webster, R. D.; Li, X., *Organometallics* **2008,** *27*, 4484-4493.
(43) Kownacki, I.; Kubicki, M.; Szubert, K.; Marciniec, B., *J. Organomet. Chem.* **2008,** *693*, 321-328.
(44) Hillier, A. C.; Lee, H. M.; Stevens, E. D.; Nolan, S. P., *Organometallics* **2001,** *20*, 4246-4252.
(45) Sargent, A. L.; Hall, M. B., *Inorg. Chem.* **1992,** *31*, 317-321.
(46) Martin, M.; Sola, E.; Torres, O.; Plou, P.; Oro, L. A., *Organometallics* **2003,** *22*, 5406-5417.
(47) Castellanos, A.; Ayllon, J. A.; Sabo-Etienne, S.; Donnadieu, B.; Chaudret, B.; Yao, W. B.; Kavallieratos, K.; Crabtree, R. H., *Comptes Rendus De L Academie Des Sciences Serie Ii Fascicule C-Chimie* **1999,** *2*, 359-368.
(48) Oldham, W. J.; Hinkle, A. S.; Heinekey, D. M., *J. Am. Chem. Soc.* **1997,** *119*, 11028-11036.
(49) Campora, J.; Lopez, J. A.; Palma, P.; del Rio, D.; Carmona, E.; Valerga, P.; Graiff, C.; Tiripicchio, A., *Inorg. Chem.* **2001,** *40*, 4116-4126.
(50) Crabtree, R., *Accounts Chem. Res.* **1979,** *12*, 331-337.
(51) Schmidt, A.; Schomäcker, R., *Ind. Eng. Chem. Res.* **2007,** *46*, 1677-1681.
(52) Moura, F. C. C.; dos Santos, E. N.; Lago, R. M.; Vargas, M. D.; Araujo, M. H., *J. Mol. Catal. A-Chem.* **2005,** *226*, 243-251.
(53) Pazderski, L., *Magn. Reson. Chem.* **2008,** *46*, S3-S15.
(54) Stott, K.; Keeler, J.; Van, Q. N.; Shaka, A. J., *J. Magn. Reson.* **1997,** *125*, 302-324.
(55) Eckert, J.; Jensen, C. M.; Koetzle, T. F.; Lehusebo, T.; Nicol, J.; Wu, P., *J. Am. Chem. Soc.* **1995,** *117*, 7271-7272.
(56) Li, S. H.; Hall, M. B.; Eckert, J.; Jensen, C. M.; Albinati, A., *J. Am. Chem. Soc.* **2000,** *122*, 2903-2910.
(57) Lenges, C. P.; Brookhart, M.; Grant, B. E., *J. Organomet. Chem.* **1997,** *528*, 199-203.
(58) Lenges, C. P.; White, P. S.; Brookhart, M., *J. Am. Chem. Soc.* **1999,** *121*, 4385-4396.
(59) Duckett, S. B.; Mewis, R. E., *Accounts Chem. Res.* **2012,** *45*, 1247-1257.
(60) Barskiy, D. A.; Kovtunov, K. V.; Koptyug, I. V.; He, P.; Groome, K. A.; Best, Q. A.; Shi, F.; Goodson, B. M.; Shchepin, R. V.; Coffey, A. M.; Waddell, K. W.; Chekmenev, E. Y., *J. Am. Chem. Soc.* **2014,** *136*, 3322-3325.
(61) Lloyd, L. S.; Asghar, A.; Burns, M. J.; Charlton, A.; Coombes, S.; Cowley, M. J.; Dear, G. J.; Duckett, S. B.; Genov, G. R.; Green, G. G. R.; Highton, L. A. R.; Hooper, A. J. J.; Khan, M.; Khazal, I. G.; Lewis, R. J.; Mewis, R. E.; Roberts, A. D.; Ruddlesden, A. J., *Catal. Sci. Technol.* **2014,** *4*, 3544-3554.
(62) Aguilar, J. A.; Adams, R. W.; Duckett, S. B.; Green, G. G. R.; Kandiah, R., *J. Magn. Reson.* **2011,** *208*, 49-57.
(63) Aguilar, J. A.; Elliott, P. I. P.; Lopez-Serrano, J.; Adams, R. W.; Duckett, S. B., *Chem. Commun.* **2007**, 1183-1185.
(64) Torres, O.; Martin, M.; Sola, E., *Organometallics* **2009,** *28*, 863-870.
(65) Lloyd, L. S.; Adams, R. W.; Bernstein, M.; Coombes, S.; Duckett, S. B.; Green, G. G. R.; Lewis, R. J.; Mewis, R. E.; Sleigh, C. J., *J. Am. Chem. Soc.* **2012,** *134*, 12904-12907.
(66) Gruber, S.; Pfaltz, A., *Angew. Chem.-Int. Edit.* **2014,** *53*, 1896-1900.
(67) Cheng, C.; Kim, B. G.; Guironnet, D.; Brookhart, M.; Guan, C.; Wang, D. Y.; Krogh-Jespersen, K.; Goldman, A. S., *J. Am. Chem. Soc.* **2014,** *136*, 6672-6683.
(68) Dolomanov, O. V.; Bourhis, L. J.; Gildea, R. J.; Howard, J. A. K.; Puschmann, H., *J. Appl. Crystallogr.* **2009,** *42*, 339-341.
(69) Sheldrick, G. M., *Acta. Crystallogr. A* **2008,** *64*, 112-122.
(70) Arduengo, A. J., *III. U.S. Patent 5077414* **1991**.

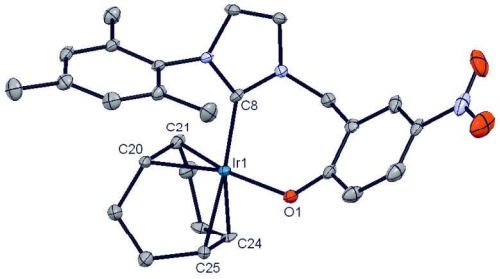

462x194mm (300 x 300 DPI)

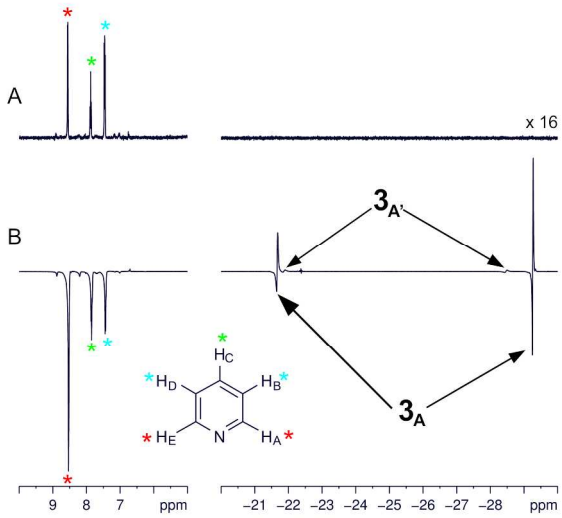

290x205mm (300 x 300 DPI)

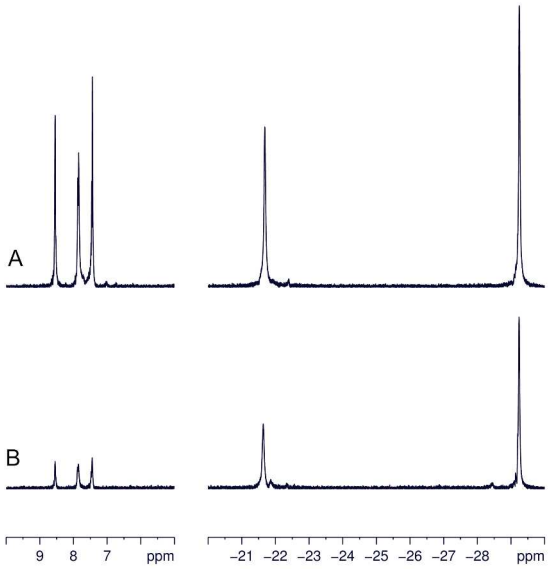

281x198mm (300 x 300 DPI)

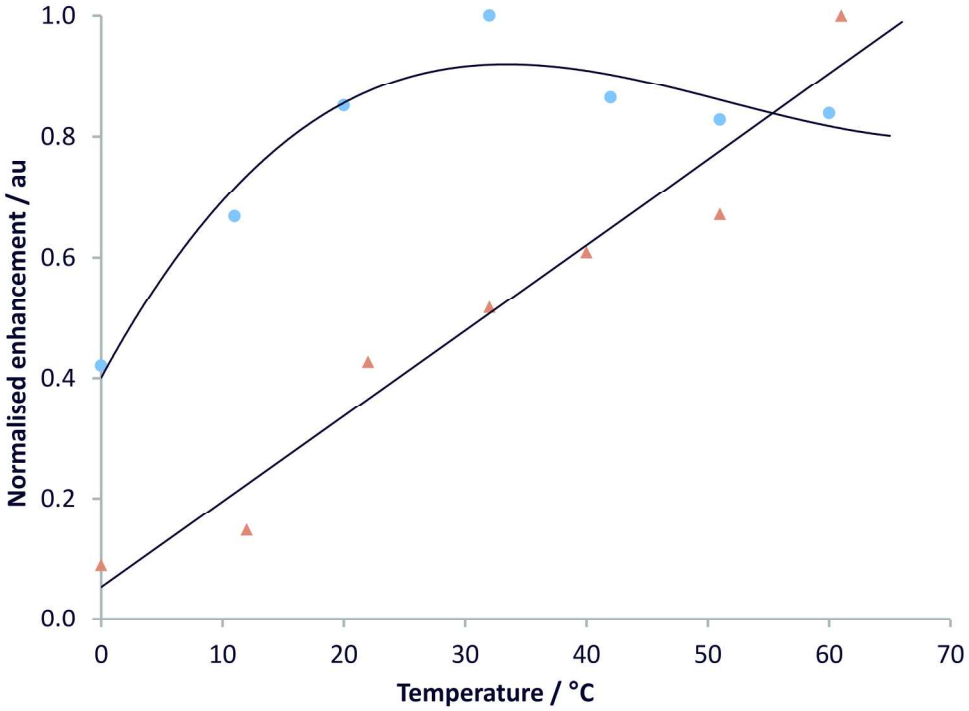

199x149mm (300 x 300 DPI)

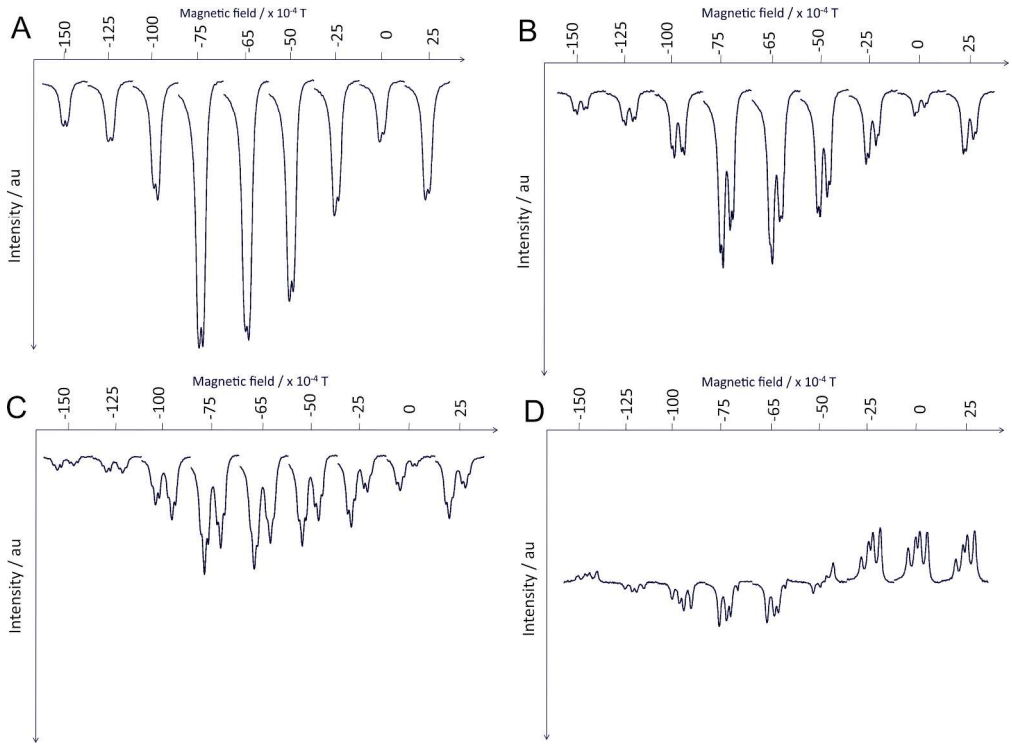

281x206mm (300 x 300 DPI)

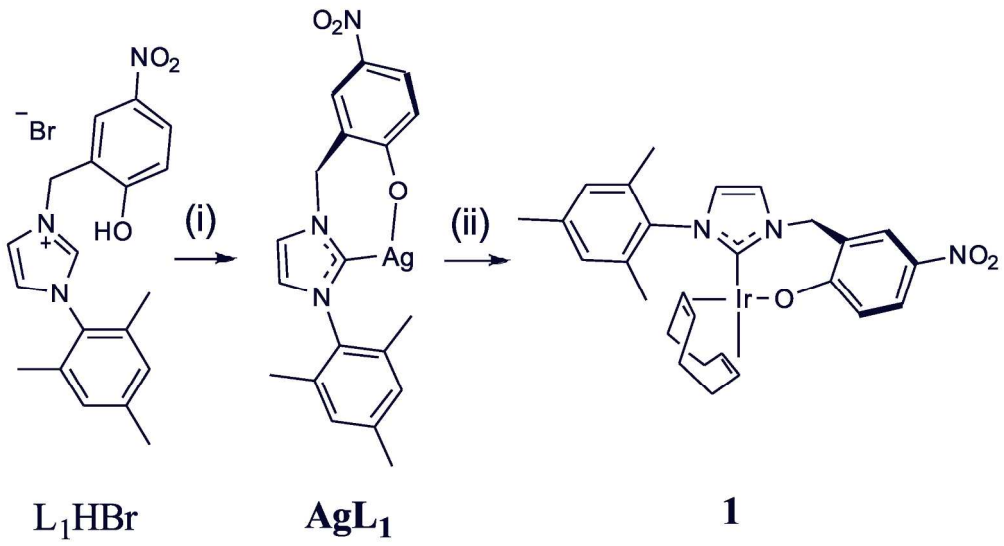

Reagents and conditions: (i) Ag_2O, THF, toluene, reflux, 3 h; (ii) $[Ir(COD)Cl]_2$, THF, r.t., 18 h

209x139mm (300 x 300 DPI)

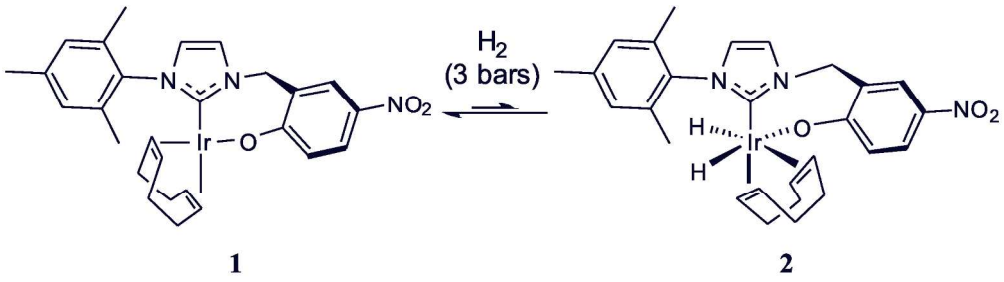

1 2

209x59mm (300 x 300 DPI)

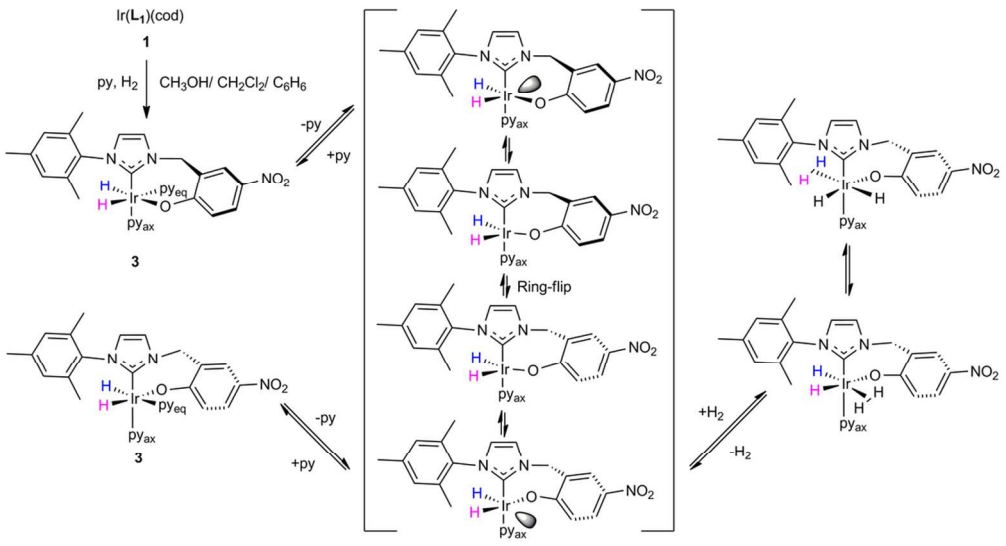

102x55mm (300 x 300 DPI)

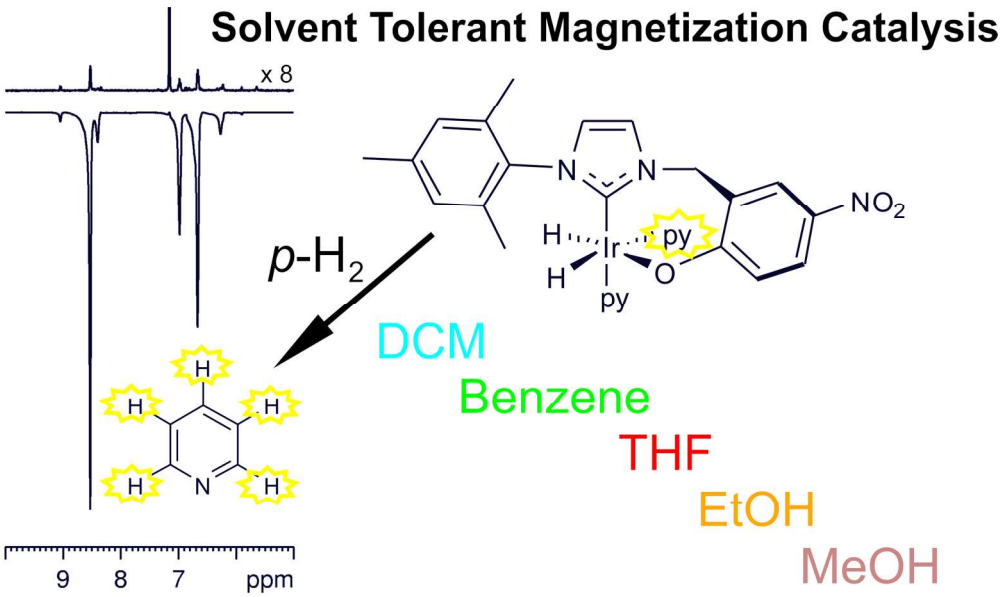

173x102mm (300 x 300 DPI)